Predicting the Energetics, Phase Stability, and Morphology Evolution of Faceted and Spherical Anatase Nanocrystals

2 AUTHORS:

Amanda S Barnard
The Commonwealth Scientific and Industrial ...
181 PUBLICATIONS   4,318 CITATIONS

SEE PROFILE

Peter Zapol
Argonne National Laboratory
139 PUBLICATIONS   4,081 CITATIONS

SEE PROFILE

Predicting the Energetics, Phase Stability, and Morphology Evolution of Faceted and Spherical Anatase Nanocrystals

A. S. Barnard*,† and P. Zapol†,‡,§

Center for Nanoscale Materials and Materials Science and Chemistry Divisions, Argonne National Laboratory, 9700 South Cass Avenue, Argonne, Illinois 60439

Inconsistencies in experimental thermochemical analysis of the anatase to rutile phase transition have led to various studies in order to elucidate the physical and chemical parameters affecting the stability of TiO_2 at the nanoscale. Using a thermodynamic model, we present predictions of the transition enthalpy of nanocrystalline anatase and rutile as a function of shape, size, and degree of surface passivation, showing that thermochemical results can differ for various faceted or spherical nanoparticles.

1. Introduction

Titanium dioxide (TiO_2) is an important accessory oxide mineral[1] widely used for a number of technological applications,[2−6] and nanoparticles of this material are proving to be very useful in advanced photochemical applications,[7] especially interfacing with organic molecules[8] such as DNA.[9] While the finite size on the nanoscale is instrumental in facilitating these new technologies, the phase and morphology have been found to be critical parameters determining their suitability for particular applications.[10−14]

Although macroscopically the rutile is the thermodynamically stable phase and the anatase phase is metastable at ambient pressures and temperatures,[15] anatase has been found to be a majority product of industrial sol−gel and aerosol syntheses of TiO_2[5] and is common in nanoscale samples.[6,16,17] The transformation from anatase to rutile is observed at different temperatures[18,19] and sizes,[20,21] depending upon experimental conditions. It has been suggested that the surface enthalpies of the anatase and rutile phases are sufficiently different that a crossover in thermodynamic stability can occur and that anatase is in fact the stable polymorph at the nanoscale.[4,17]

Gribb and Banfield[5] and later Zhang and Banfield[4] determined that the synthesis of nanocrystalline TiO_2 consistently resulted in anatase nanoparticles, which transformed to rutile upon reaching a particular size (<14 nm) and that, once formed, the rutile crystals grew considerably faster. It was pointed out by Hwu and colleagues[22] that the relative stability of anatase and rutile was also dependent on the synthesis technique, and reported anatase <50 nm transforming to rutile at ∼973 K.

The energetics of anatase and rutile were first measured using high-temperature oxide melt solution calorimetry by Navrotsky and Kleppa.[6] They obtained the enthalpy for the bulk phase transformation (via extrapolation) of 6.57 ± 0.79 kJ/mol at 968 K and concluded that bulk anatase was metastable (with respect to bulk rutile) under all temperature−pressure conditions. Mitsuhashi and Kleppa[16] determined the enthalpy of the anatase to rutile phase transformation for hydrothermally prepared

anatase by using high-temperature oxide melt solution calorimetry and differential scanning calorimetry (DSC) to be 3.26 ± 0.84 and 2.93 ± 1.26 kJ/mol, respectively. In both studies, the water contents, the impurities, and the exact size of the particles were not reported.

Rao[23] estimated the enthalpy of the anatase to rutile phase transformation to be 0.42 ± 0.21 kJ/mol at 1176 K, using DTA with spectroscopically pure anatase of ∼40 nm in diameter. Margrave and Kybett[24] reported a transformation enthalpy of 8.37 ± 5.92 kJ/mol obtained with fluorine combustion calorimetry. Most recently Rande et al.[25] measured the energetics of anatase and rutile using high-temperature oxide melt drop solution calorimetry at 975 K with $3Na_2O \cdot 4MoO_3$ solvent and a Calvet twin microcalorimeter. The study investigated the effects of particle size and adsorbed water, and concluded bulk anatase is 2.61 ± 0.41 kJ/mol higher in enthalpy than bulk rutile.

It has been proposed by a number of authors that the anatase to rutile phase transformation is dependent not only on grain size but also on impurities, reaction atmosphere, and synthesis conditions.[26−31] Zhang and Banfield[27,32] suggested that the mechanism of the anatase to rutile phase transformation was temperature dependent; with the transformation being dominated by interface nucleation <873 K, by both interface and surface nucleation at 873−1273 K, and by bulk nucleation >1273 K. Yang et al.[30] showed that synthesis conditions (chemicals/ peptizing agents) affect the crystallinity and phase transition temperature. In this vein, Zaban et al.[31] noted that the surface structure of TiO_2 is affected by the preparation conditions, and Ahonen et al.[33] observed that anatase synthesized in air transformed to rutile at 973 K but anatase synthesized in nitrogen transformed to rutile at 1173 K. The phase transition was also found to be affected by doping with manganese ions,[34] niobium,[35] and cesium dioxide,[36] and it occurred at a higher temperature with the addition of SiO_2.[28,29]

It is possible that nanocrystal morphology is also a factor affecting the phase stability as, contrary to numerous assumptions, anatase nanoparticles are not necessarily spherical.[37] For example, high-resolution transmission electron microscopy (HRTEM) micrographs of Penn and Banfield[38] clearly show that the tetragonal bipyramidal morphology persists down to sized of 3−5 nm. However, the thermodynamic and kinetic factors controlling the development of various crystal faces in

---

* E-mail: amanda.barnard@anl.gov.
† Center for Nanoscale Materials, Argonne National Laboratory.
‡ Materials Science and Chemistry Divisions, Argonne National Laboratory.
§ E-mail: zapol@anl.gov.

the nanocrystalline powders are unknown. The studies described above indicate that the fraction of various crystallographic surfaces may vary depending upon the preparation conditions. The surface enthalpies derived from the calorimetric data[25] represent the averaged surface enthalpy and give no indication of the abundance of a particular surface (or morphology). It has been suggested by others[25] that the range in values of the nanocrystalline anatase calorimetric data may reflect differences in nanocrystal morphology, rather than purely random statistical factors.

This question may be investigated using a suitable thermodynamic treatment that encompasses the morphological characteristics of nanocrystals as well as their size and accounts for the surface terminations resulting from various synthesis conditions. Recently, we have developed a thermodynamic model capable of describing the shape of nanoparticles as a function of size,[39] and we have successfully applied it to titanium dioxide nanoparticles, with particular attention given to the anatase to rutile phase transition. The same model has also been successfully applied to titanium dioxide nanoparticles with hydrogenated surfaces, to investigate the effects of surface passivation on the equilibrium shape and the phase transition, and has shown that surface passivation has an important impact on nanocrystal morphology and phase stability.[40]

The aims of the present study are to determine whether the shape of nanocrystalline TiO_2 differs from the macroscopic Wulff construction and to investigate whether differences in nanomorphology may account for the variations in (anatase-to-rutile) transition energies and sizes measured in the calorimetric experiments of other authors. Section 2 outlines the shape dependent thermodynamic model and the computational method used to calculate the input parameters. This is followed in section 3 by an analysis of the optimized shape of TiO_2 nanoparticles as a function of surface hydrogenation and results of the transition energetics of various shaped anatase and rutile nanocrystals. Finally, for an explicit case (the anatase truncated bipyramid), the sensitivity of the transition energetics to variations in nanomorphology is also highlighted in section 3.

2. Determining the Free Energy of Formation

2.1. Thermodynamic Model. For a given nanoparticle of material x, the free energy may be expressed as a sum of contributions from the particle bulk and surfaces, such that

$$G_x{}^o = G_x{}^{bulk} + G_x{}^{surface} \tag{1}$$

The free energy of formation of a nanocrystal $G_x{}^o$ is defined[39] in terms of the surface energy γ_{xi} for each surface i, weighted by the factors f_i, such that $\Sigma_i f_i = 1$. Hence,

$$G_x{}^o = \Delta_f G_x{}^o + \frac{M}{\rho_x}(1 - e)\left[q\sum_i f_i \gamma_{xi}\right] \tag{2}$$

where $\Delta_f G_x{}^o$ is the standard free energy of formation of the bulk (macroscopic) material, M is the molar mass, ρ_x is the density and e is the volume dilation induced by the surface tension (which cannot be ignored at the nanoscale). In general, the surface-to-volume ratio q and the weighting factors f_i must be calculated explicitly for each shape and the facets therein. In this model, the size dependence is introduced not only by the reduction of e as the crystal grows larger but by also the surface-to-volume ratio q. The shape dependence is also introduced by q, as well as the weighted sums of the surface

energies and the surface tension, corresponding to the surfaces present in the particular morphology of interest.

The value of γ was calculated from the energy per TiO_2 unit for the bulk (E^{bulk}) and the total energy of the surface ($E_N{}^{surface}$) slabs using the expressions

$$\gamma = \frac{G}{A} \tag{3}$$

$$G = \frac{1}{2}(E_N{}^{surface} - NE^{bulk} - N_H E^H) \tag{4}$$

where G is the free energy of the slab surface, A is the area of the surface, and N is the number of TiO_2 units in the (stoichiometric) cell. E^{bulk} was obtained from highly accurate, large-scale periodic super-cell calculations, under the same computational conditions. This method has been used successfully before.[40] To account for the surface hydrogenation, N_H is the number of terminating hydrogen atoms present on the slab, and $E^H = {}^1/_2 E(H_2)$ is half the energy of a free H_2 molecule calculated using the same ab initio method.

The volume dilation due to the surface tension σ (which has a small but important effect on the calculation of the anatase to rutile phase transition[41]) may be approximated using the Laplace−Young equation[39] for the effective pressure

$$P_{eff} = \frac{2\sigma_x}{R} \tag{5}$$

where R is the radius of the particle; so that in general (with the compressibility $\beta = 1/B_0$, with B_0 the zero pressure bulk modulus)

$$e = \frac{2\beta\sigma_x}{R} \tag{6}$$

The surface tension is approximated by summing over the (weighted) surface tension of the crystallographic surfaces present on the nanocrystal

$$\sigma_x = \sum_i f_i \sigma_{xi} \tag{7}$$

The value of σ was obtained using the expression

$$\sigma = \frac{\partial G}{\partial A} \approx \frac{\Delta G}{\Delta A} \tag{8}$$

By application of a two-dimensional uniform dilation in the plane of the surface (including full optimization of internal parameters) and calculation of the free energy G as indicated in eq 4 for each area, the change in free energy (ΔG) was approximated for a set of area dilations (ΔA). After these results were plotted, an estimate of the surface tension was obtained from the slope.

The values of β for anatase and rutile were previously determined by fitting our calculated energy vs volume curves to the Vinet equation of state.[42] The resulting values of the zero pressure bulk modulus for anatase of 190 GPa and rutile for 218 GPa were in good agreement with the experimental values of 179 GPa measured by Arlt et al.[43] and of 211 GPa measured by Gerward and Olsen,[44] respectively.

We have previously shown that the Laplace−Young description of the pressure is suitable in the case of faceted nanocrystals and that the edge and corner effects are most important below diameters of approximately 2 nm.[40,45] Therefore, the surface energies and surface tensions for each surface facet i, along with

Anatase Nanocrystals

J. Phys. Chem. B, Vol. 108, No. 48, 2004 **18437**

TABLE 1: Comparison of Surface Free Energy γ and Surface Tension σ (in J/m²) Calculated Using Density Functional Theory,[40] for the Stable Clean, Partially Hydrogenated, and Fully Hydrogenated Low Index Surfaces of Anatase and Rutile

	anatase					
	clean		partial		full	
	γ	σ	γ	σ	γ	σ
(001)	0.51	2.07	0.86	0.50	0.84	0.91
(100)	0.39	0.60	0.55	0.23	0.65	−0.19
(101)	0.35	0.51	0.51	0.71	0.63	0.09

	rutile					
	clean		partial		full	
	γ	σ	γ	σ	γ	σ
(100)	0.60	0.95	0.71	0.66	1.82	0.80
(110)	0.47	1.25	0.56	1.96	0.84	1.27
(011)	0.95	1.50	1.02	0.39	1.19	1.38

the molar mass of TiO_2, the density of anatase and rutile ($\rho_{\mathscr{A}}$ = 3.893 g/cm³ and $\rho_{\mathscr{R}}$ = 4.249 g/cm³) and the standard free energies of formation[46] ($\Delta_f G^o{}_{\mathscr{A}}$ and $\Delta_f G^o{}_{\mathscr{R}}$) are all that is required to compare the phase stability of faceted TiO_2 nanocrystals over this size.

2.2. Ab Initio Methods. The energetics of the low index surfaces of rutile and anatase (i = (100), (101)/(011), (110), and (001)) were investigated by comparing highly accurate first principles calculations of the total energy of two-dimensional slabs with the corresponding bulk energy. The clean (vacuum-terminated) slabs were generated by the addition of a 15 Å vacuum layer in the crystallographic plane of interest, whereas the H-terminated slabs were generated by the addition of a 10 Å vacuum layer in the desired plane and then either fully or partially hydrogenating the "cleaved" surfaces. The fully hydrogenated surfaces were obtained by terminating all under-coordinated sites (both Ti and O atoms) with hydrogen atoms, whereas the partially hydrogenated surfaces were obtained by terminating only the under-coordinated bridging O atoms with hydrogen. Each surface slab was relaxed prior to calculation of the total energy.

Previously, our calculations were carried out using density functional theory (DFT) within the generalized-gradient approximation (GGA), with the exchange-correlation functional of Perdew and Wang (PW91).[47] These calculations were implemented using the Vienna ab initio simulation package (VASP)[48,49] and the projected augmented wave (PAW) potentials[50] and are described in detail in ref 40.

2.3. Surface Energy and Surface Tension. The thermodynamic sequence (101) < (100) < (001) for the clean surface was found to be the same for the partially hydrogenated and fully hydrogenated anatase surfaces,[40] as indicated by Table 1. The effects of hydrogenation on the surface tension σ of anatase varied considerably with degree of hydrogenation. For example, the surface tension of the fully hydrogenated (100) surface was even found to be negative, indicating the tendency for this surface to expand (rather than contract) and, if present on the surface of a nanocrystal, produce a tensile dilation in the direction of the surface normal.

In general the surface energies γ for the rutile surfaces (see Table 1) are increased by surface hydrogenation. In this case, the sequences of (110) < (100) < (011) for the clean surfaces,[40] (110) < (100) < (011) for the partially hydrogenated surfacesm[40] and (110) < (011) < (100) for the fully hydrogenated surfaces[40] were obtained. Like anatase, the σ of the rutile surfaces is sensitive to the degree of hydrogenation, although
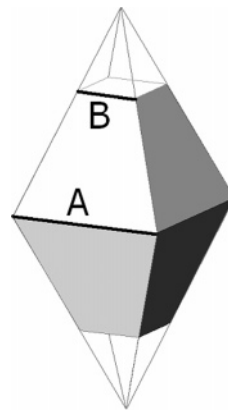
Figure 1. Example of the anatase tetragonal {101} bipyramid is shown in outline, and an example of the bifrustum formed by addition of (001) and (00$\bar{1}$) truncation facets is shown as the interior solid. The side lengths labeled **A** and **B** are used to define the degree of truncation.

the surface tensions of the clean and fully hydrogenated surfaces are closer in magnitude than that of the partially hydrogenated surface.

3. Results and Discussion

3.1. Nanomorphology of Anatase and Rutile. Initially, the shapes of the anatase and rutile nanocrystals compared in this study were determined by generating the Wulff construction[51−53] for each material, using surface energies listed in Table 1. However, as the Wulff construction does not take into account the effects of surface tension, it is possible that the morphologies of nanocrystals may deviate from this shape. In the case of anatase, since the nanocrystal morphology is represented by a closed form, the thermodynamic model outlined above may also be used to minimize the free energy as a function of shape and thereby determine the optimized shape of anatase nanocrystals.

Beginning with the bipyramid (wire frame in Figure 1) as the limiting case, the morphology of anatase nanocrystals has been defined in terms of two independent length parameters **A** and **B**, as shown in Figure 1. The side of this bipyramid is denoted **A**. In nature, anatase crystals often exhibit a truncated bipyramid, or bifrustum, with square facets in the (001) and (00$\bar{1}$) planes (displayed as the interior solid in Figure 1). The side of this "truncation" facet is denoted **B**. The degree of truncation has therefore been described by the size of **B** with respect to **A** (where $0 \leq \mathbf{B} \leq \mathbf{A}$).

By defining all the geometric parameters such as the volume and surface area of the various facets in terms of the ratio **B/A**, the energy was minimized with respect to this new variable. The numerical minimization was performed using a conjugate gradient scheme, in an attempt to find a value of **B/A** that produces a shape that is lower in energy than the Wulff construction as a function of size. This procedure was performed for clean, partially hydrogenated, fully hydrogenated anatase nanocrystals.

Figure 2 shows a plot of the optimized **B/A** for sizes **A** = 0 to 300 nm. At very small sizes the clean anatase nanocrystals (in a vacuum) are predicted to be a tetragonal bifrustum with a truncation facet of side length **B** ≈ 0.32 **A**, even though the Wulff construction (with same energies) predicts shape where **B** = 0.47 **A**. When the surfaces are partially hydrogenated the shape is also predicted to be a tetragonal bifrustum but with a truncation facet of side length **B** ≈ 0.26 **A**, and when fully hydrogenated the bifrustum has truncation facet with a side length **B** ≈ 0.34 **A**. As the anatase crystals increase in size, and the effects of surface tension and the need for the shape to
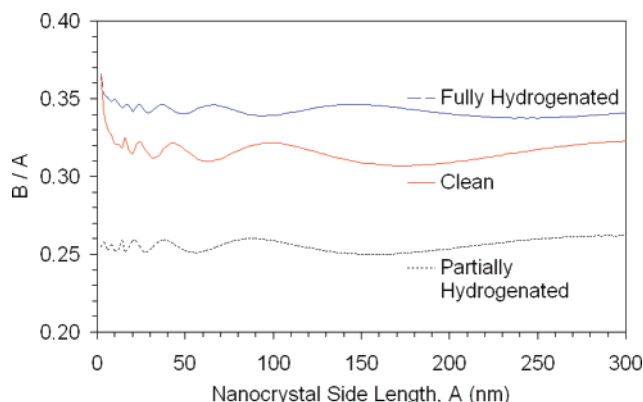
Figure 2. Plot of the optimized ratio **B/A**, for anatase nanocrystals with clean, partially hydrogenated and fully hydrogenated surfaces, with a side length **A** = 0 to 300 nm. The facet edges **A** and **B** are defined in Figure 1.
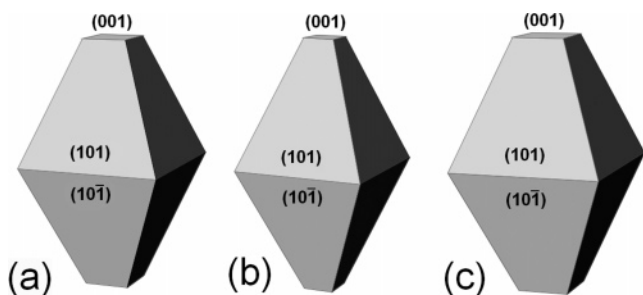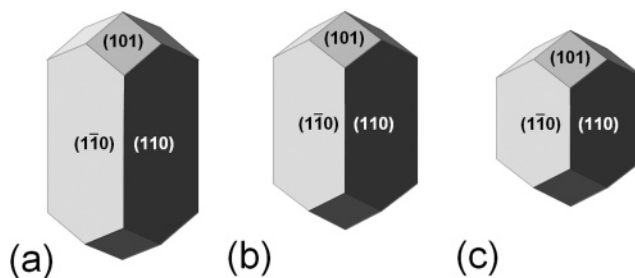

Figure 3. Optimized shaped of anatase nanocrystals with (a) clean, (b) partially hydrogenated, and (c) fully hydrogenated surfaces, calculated using the surface free energies listed in Table 1.

Figure 4. Lowest energy shapes, which were found to be the Wulff constructions for rutile with (a) clean, (b) partially hydrogenated, and (c) fully hydrogenated surface, calculated using the surface free energies listed in Table 1.

TABLE 2: Comparison of the Approximate Anatase-to-Rutile Phase Transition Sizes for Clean, Partially Hydrogenated, and Fully Hydrogenated Nanocrystals[a]

| anatase	clean	partial	full
TiO_2 units	12300	10800	196900
average diameter (nm)	9.3	8.9	23.1
apical length (nm)	19.9	19.1	49.8
rutile	clean	partial	full
TiO_2 units	12300	10800	196900
average diameter (nm)	9.0	8.6	22.2
apical length (nm)	13.3	10.4	41.2

[a] Note that the average diameter and apical (apex-to-apex) length varies since shape of the nanocrystals is dependent on the degree of surface hydrogenation.

minimize the surface-to-volume ratio diminish, the shape converges to that of the Wulff construction which remains the macroscopically lowest energy shape. Note that this convergence occurs at sizes larger than those shown in Figure 2, at approximately 10^8 TiO_2 units.

Unfortunately this procedure may not be applied to rutile, since the rutile tetragonal {110} prism represents an open form. Optimization of the prism ratio leaves the system free to become one-dimensional nanowires, which may not be realistic. Although both acicular crystals and blocky habits are observed in rutile crystals microscopically and macroscopically, it cannot be assured that an aspect ratio predicted by the model is physically significant. However (as a brief check), a number of aspect ratios were tested for rutile nanocrystals using the thermodynamic model, and the Wulff construction was consistently found to correspond to the lowest energy shape for a given number of atoms. Therefore, the results show that clean rutile surfaces produce longer prismatic crystals, whereas the crystals become more stunted as the coverage of surface hydrogen is increased.[40]

Thus, the shapes shown in Figures 3 and 4 correspond to the minimum energy morphology calculated in this study for clean, partially hydrogenated and fully hydrogenated surfaces.

3.2. Transition Energetics. For each of the nanocrystals described above, the value of $G°_{\mathscr{A}}$ and $G°_{\mathscr{R}}$ were calculated and plotted as functions of the number of TiO_2 units. By determination of each point of intersection, the phase stability of the faceted nanocrystals has been determined.[40] These results, for the optimized morphologies, are contained within Table 2. Experimentally, the transition point at $\sim$650−800 K has been predicted to be at approximately 11.4−17.6 nm (for hydrothermal samples), but it has been found to decrease with temperature.[5]

In the treatment used herein the thermodynamic phase stability is described by the Gibbs free energy ($\Delta G = \Delta H - T\Delta S$) rather than the enthalpy. As the calculations presented here have been performed at $T = 0$, the free energy and enthalpy are equivalent. If temperature effects were to be considered, available low-temperature heat capacity and entropy data of fine-grained anatase and rutile[16] suggest that rutile and anatase have the same entropy within experimental error ($S°$(298 K, $\mathscr{A}$) = 49.9 ± 0.3 J/mol·K and $S°$(298 K, $\mathscr{R}$) = 50.6 ± 0.6 J/mol·K[54]). Thus, the $T\Delta S$ will not significantly perturb the sequence of stability seen from the enthalpies.

Therefore, the Gibbs free energy may also be used as a measure of the enthalpy of formation.[25] By subtracting the enthalpy of formation for bulk rutile (where we assume $\Delta H°_{\mathscr{R}} = \Delta G°_{\mathscr{R}}$), and plotting as a function of the surface to volume ratio q, a theoretical approximation may be made of the transition enthalpies of anatase and rutile nanocrystals (with respect to bulk rutile) that are comparable with the oxide melt calorimetry results of Rande et al.[25] This procedure has been performed for nanocrystals of anatase and rutile with clean, partially hydrogenated, and fully hydrogenated surfaces, as shown in Figures 5, 6, and 7, respectively.

In the case of the "spherical" particles, a spherical shape was programmed into the model and the surface energy and surface tension was taken as an average of those calculated for low index surfaces.[4] It is important to note that the addition of higher index (higher energy) surfaces may result in an increase in the predicted energy for this shape; therefore, the result for the "spheres" here represents a lower estimate.

Upon examination of Figures 5−7, the first aspect that is apparent is that the degree of surface hydrogenation has an important impact on the transition enthalpy. This is consistent with the results mentioned above for the transition sizes for clean and hydrogenated nanocrystals,[40] with phase transition enthalpies predicted at 13.7, 21.9, and 15.1 kJ/mol for the clean, partially hydrogenated, and fully hydrogenated nanocrystals, respectively. Note that the bulk anatase to bulk rutile transition enthalpy

Anatase Nanocrystals

J. Phys. Chem. B, Vol. 108, No. 48, 2004 **18439**
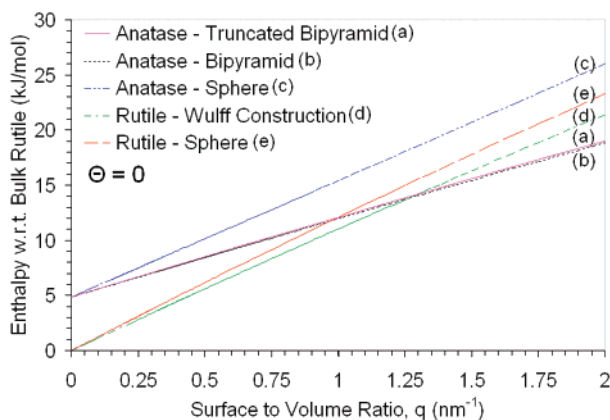
Figure 5. Calculated enthalpy of faceted and spherical TiO_2 nano-particles with clean surfaces ($\Theta = 0$). The faceted shapes (bifrustum for anatase and Wulff construction for rutile) correspond to those shown in Figures 3 and 4, respectively.
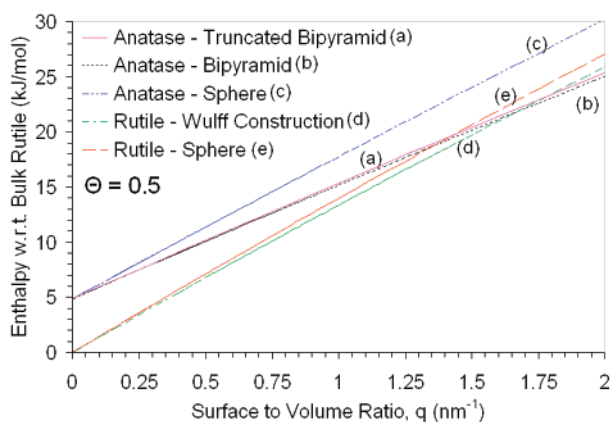
Figure 6. Calculated enthalpy of faceted and spherical TiO_2 nano-particles with partially hydrogenated surfaces ($\Theta = 0.5$). The faceted shapes (bifrustum for anatase and Wulff construction for rutile) correspond to those shown in Figures 3 and 4, respectively.
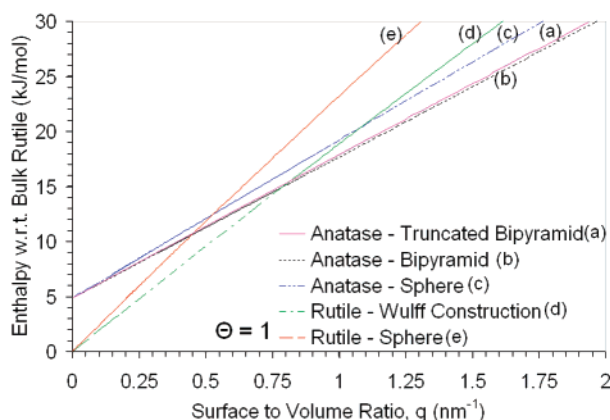
Figure 7. Calculated enthalpy of faceted and spherical TiO_2 nano-particles with fully hydrogenated surfaces ($\Theta = 1$). The faceted shapes (bifrustum for anatase and Wulff construction for rutile) correspond to those shown in Figures 3 and 4, respectively.

(indicated by the convergence of the anatase results as $q \rightarrow 0$) of 4.85 kJ/mol is a result of the difference $\Delta G^{\circ}_{\mathcal{A}} - \Delta G^{\circ}_{\mathcal{R}}$ from the JANAF tables.[46]

It is also clear from Figures 5−7 that spherical TiO_2 nanoparticles (both anatase and rutile) represent a higher energy shape and are therefore not as thermodynamically favorable as faceted nanocrystals. For this reason, it is less likely that spherical nanoparticles will form without some perturbation to
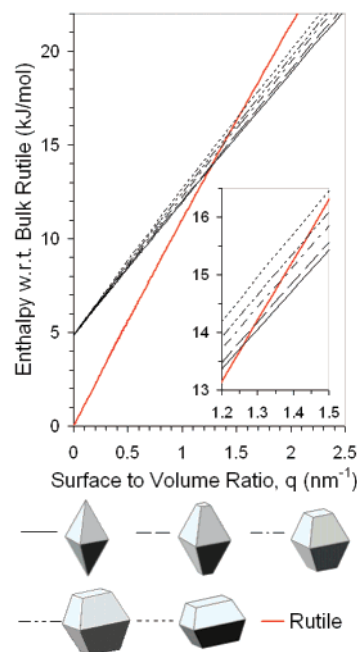
Figure 8. Calculated enthalpy of clean anatase nanocrystals (with respect to bulk rutile) as a function of degree of truncation, showing the resulting change in the anatase to rutile phase transition size and energetics. The anatase nanocrystals correspond to **B/ A** = 0.0 (perfect bipyramid), 0.3, 0.5, 0.6 and 0.8, as shown in the legend.

the system, and the probability of sphere-to-sphere transitions is low. In the case of the partially hydrogenated nanocrystals, the anatase-sphere to rutile-sphere transition is thermodynami-cally forbidden. However, the possibility of a transition between faceted anatase and spherical rutile nanoparticles is increased by surface hydrogenation. When the surfaces are fully hydro-genated, the difference in transition enthalpy between a faceted anatase to faceted rutile transition and a faceted anatase to spherical rutile transition is approximately −4.6 kJ/mol.

3.3. Energetics as a Function of Truncation. Finally, the effects of truncating the nanocrystal apex may also be inves-tigated using Equation 2. By changing the geometric parameters of the model, facets in the (001) plane may be introduced at a desired degree of truncation, and the corresponding $G^{\circ}_{\mathcal{A}}$ plotted as a function of q. This has been performed for a number of truncations, as shown in Figure 8, showing that the transition size decreases but the transition enthalpy increases with trunca-tion. The degree of truncation of the anatase nanocrystals shown in the legend of the graph varies from **B/A** = 0.0, 0.3, 0.5, 0.6 and 0.8.

As indicated by Figure 8, varying the truncation of the anatase nanocrystals introduces a spread, both in the energetics and the size of the phase transition, that may help to explain some of the inconsistencies and variation in the experimental results of the authors mentioned above.

4. Conclusions

In conclusion, not only does surface passivation affect the thermochemistry of the phase transition, as proposed by other authors[30,31,33] and supported by the results of hydrogenated surfaces outlined above, but also shape may play an important part. Using a thermodynamic model, we have presented predic-tions of the transition enthalpy of nanocrystalline anatase and rutile as a function of shape, size, and degree of surface hydrogenation, showing that transition enthalpies may differ as a result of morphological changes and surface structure.

Although spherical TiO_2 nanoparticles do not represent a minimum energy morphology, a phase transition from faceted anatase nanocrystals to spherical rutile nanoparticles may occur, albeit at larger particle sizes. Further, our results indicate that the energy and particle size required for this (and other) transitions may be controlled by altering the degree of surface passivation.

Therefore, inconsistencies in experimental evidence concerning the anatase to rutile may be explained not only by impurities and synthesis conditions[27-31] but also by variations in the nanoparticle shapes. Further work is underway to determine the effects of water on the anatase to rutile phase transition, the nanoparticle morphology, and the thermochemistry of the systems.

References and Notes

(1) Banfield, J. F.; Bischoff, B. L.; Anderson, M. A. *Chem. Geol.* **1993**, *110*, 211.

(2) Zhang, H.; Finnegan, M.; Banfield, J. F. *Nano Lett.* **2001**, *1*, 81.

(3) Elder, S. H.; Cot, F. M.; Su, Y.; Heald, S. M.; Tyryshkin, A. M.; Bowman, M. K.; Gao, Y.; Joly, A. G.; Balmer, M. L.; Kolwaite, A. C.; Magrini, K. A.; Blake, D. M. *J. Am. Chem. Soc.* **2000**, *122*, 5138.

(4) Zhang, H.; Banfield, J. F. *J. Mater. Chem.* **1998**, *8*, 2073.

(5) Gribb, A. A.; Banfield, J. F. *Am. Mineral.* **1997**, *82*, 717.

(6) Navrotsky, A.; Kleppa, O. J. *J. Am. Ceram. Soc.* **1976**, *50*, 626.

(7) Zhang, W. F.; Zhang, M. S.; Yin, Z.; Chen, Q. *Appl. Phys. B: Laser Opt.* **2000**, *70*, 261.

(8) Rajh, T.; Chen, L. X.; Lucas, L.; Liu, T.; Thurnauer, M. C.; Tiede, D. M. *J. Phys. Chem. B* **2002**, *106*, 10543.

(9) Paunesku, T.; Rajh, T.; Wiederrecht, G.; Maser, J.; Vogt, S.; Stojićević, N.; Protić, M.; Lai, B.; Oryhon, J.; Thurnauer, M.; Woloschak, G. *Nature Materials* **2003**, *2*, 343.

(10) Chen, L. C.; Rajh, T.; Jäger, W.; Nedeljkovic, J. M.; Thurnauer, M. C. *J. Synchrotron. Rad.* **1999**, *6*, 455.

(11) Rajh, T.; Nedeljkovic, J. M.; Chen, L. C.; Poluektov, O.; Thurnauer, M. C. *J. Phys. Chem. B* **1999**, *103*, 3515.

(12) Zhang, H.; Penn, R. L.; Hamers, R. J.; Banfield, J. F. *J. Phys. Chem. B* **1999**, *103*, 4656.

(13) Jang, K. D.; Kim, S.-K.; Kim, S.-J. *J. Nanoparticle Res.* **2001**, *3*, 141.

(14) Bullen, H.; Garrett, S. *Nano Lett.* **2002**, *2*, 739.

(15) Muscat, J.; Swamy, V.; Harrison, N. M. *Phys. Rev. B* **2002**, *65*, 224112.

(16) Mitsuhashi, T.; Kleppa, O. J. *J. Am. Ceram. Soc.* **1979**, *62*, 356.

(17) Zhang, H. Z.; Banfield, J. F. *J. Phys. Chem. B* **2000**, *104*, 3481.

(18) Gourma, P. I.; Mills, M. J. *J. Am. Ceram. Soc.* **2001**, *84*, 619.

(19) Li, Y.; White, T.; Lim, S. H. *Rev. Adv. Mater.* Sci. **2003**, *5*, 211.

(20) Ghosh, T. B.; Dhabal, S. *J. Appl. Phys.* **2003**, *94*, 4577.

(21) Navrotsky, A. Thermochemistry of Nanomaterials In *Nanoparticles and the Environment, Reviews in Mineralogy Geochemistry*; Banfield, J. F., Navrotsky, A., Eds., Mineralogical Society of America: Washington, DC, 2001; Vol. 44.

(22) Hwu, Y.; Yao, Y. D.; Cheng, N. F.; Tung, C. Y.; Lin, H. M. *Nanostruct. Mater.* **1997**, *9*, 355.

(23) Rao, C. N. R. *Can. J. Chem.* **1961**, *39*, 498.

(24) Margrave, J. L.; Kybett, B. D. *Technol. Rep. No. AFMO-TR-65*, Air Force Materials Laboratory, Research and Technology Division, Air Force Systems Comm, Wright-Patterson Air Force Base: Fairborn, OH, 1965; p 123.

(25) Re, M. R.; Navrotsky, A.; Zhang, H. Z.; Banfield, J. F.; Elder, S. H.; Zaban, A.; Borse, P. H.; Kulkarni, S. K.; Doran, G. S.; Whitfield, H. J. *Proc. Natl. Acad. Sci. U.S.A.* **2002**, *99*, 6481.

(26) Kittaka, S.; Matsuno, K.; Takahara, S. *J. Solid. State. Chem* **1997**, *132*, 447.

(27) Zhang, H. Z.; Banfield, J. F. *J. Mater. Res.* **2000**, *15*, 437.

(28) Yoshinaka, M.; Hirota, K.; Yamaguchi, O. *J. Am. Ceram. Soc.* **1997**, *80*, 2749.

(29) Okada, K.; Yamamoto, N.; Kameshima, Y.; Yasumori, A. *J. Am. Ceram. Soc.* **2001**, *84*, 1591.

(30) Yang, J.; Mei, S.; Ferreira, J. M. F. *J. Am. Ceram. Soc.* **2000**, *83*, 1361.

(31) Zaban, A.; Aruna, S. T.; Tirosh, S.; Gregg, B. A.; Mastai, Y. *J. Phys. Chem. B* **2000**, *104*, 4130.

(32) Zhang, H.; Banfield, J. F. *Am. Mineral.* **1999**, *84*, 528.

(33) Ahonen, P. P.; Kauppinen, E. I.; Joubert, J. C.; Deschanvres, J. L.; Van Tendeloo, G. *J. Mater. Res.* **2000**, *14*, 3938.

(34) Arroyo, R.; Córdoba, G.; Padilla, J.; Lara, V. H. *Mater. Lett.* **2002**, *54*, 397.

(35) Arbiol, J.; Cerdà, J.; Dezanneau, G.; Cirera, A.; Peiró, F.; Cornet, A.; Morante, J. R. *J. Appl. Phys.* **2002**, *92*, 853.

(36) Francisco, M. S. P.; Mastelaro, V. R. *Chem. Mater.* **2002**, *14*, 2514.

(37) Gao, Y.; Elder, S. A. *Mater. Lett.* **2000**, *44*, 228.

(38) Penn, R. L.; Banfield, J. F. *Geochim. Cosmochim. Acta* **1999**, *63*, 1549.

(39) Barnard, A. S.; Zapol, P. *J. Chem. Phys.* **2004**, *121*, 4276.

(40) Barnard, A. S.; Zapol, P. *Phys. Rev. B* **2004**, in press.

(41) Lu, H. M.; Zhang, W. X.; Jiang, Q. *Adv. Eng. Mater.* **2003**, *5*, 787.

(42) Vinet, P.; Rose, J. H.; Ferrante, J.; Smith, J. R. *J. Phys. (Paris): Condes. Matter.* **1989**, *1*, 1941.

(43) Arlt, T.; Bermejo, M.; Blanco, M. A.; Gerward, L.; Jiang, J. Z.; Staun Olsen, J.; Recio, J. M. *Phys. Rev. B* **2000**, *61*, 14414.

(44) Gerward, L.; Olsen, J. S. *J. Appl. Crystallogr.* **1997**, *30*, 259.

(45) Note that for nanoparticles less than approximately 2 nm it is preferable to make direct calculations in isolated finite structures (using suitable computational methods), since edge and corner effects will contribute more significantly to the total free energy.

(46) The experimental free energies of formation of anatase [rutile] $\Delta_f G^{\circ}_{\mathscr{A}}$ [$\Delta_f G^{\circ}_{\mathscr{R}}$] taken from the JANAF tables have been applied here, such that $\Delta_f G^{\circ}_{\mathscr{A}} = -9.491471 \times 10^{-2}$ mJ/mol [$\Delta_f G^{\circ}_{\mathscr{R}} = -9.539962 \times 10^{-2}$ mJ/mol]. Chase, M. W.; Davies, C. A.; Downey, J. R.; Frurip, D. J.; McDonald, R. A.; Syverud, A. N. *J. Phys. Chem. Ref. Data* **1985**, *14* (Suppl. 1), 1680.

(47) Perdew, J.; Wang, Y. *Phys. Rev. B* **1992**, *45*, 13244.

(48) Kresse, G.; Hafner, J. *Phys. Rev. B* **1993**, *47*, RC558.

(49) Kresse, G.; Hafner, J. *Phys. Rev. B* **1996**, *54*, 11169.

(50) Blöchl, P. E. *Phys. Rev. B* **1994**, *50*, 17953.

(51) Wulff, G. Z. *Kristallogr. Mineral* **1901** *34*, 449.

(52) Oliver, P. M.; Watson, G. W.; Kelsey, E. T.; Parker, S. C. *J. Mater. Chem.* **1997**, *7*, 563.

(53) Lazzeri, M.; Vittadini, A.; Selloni, A. *Phys. Rev. B* **2001**, *63*, 155409.

(54) Robie, R. A.; Hemingway, B. S. *U. S. Geol. Surv. Bull.* **1995**, *2131*.